A Numerical Method for a Second-Gradient Theory of Incompressible Fluid Flow

Tae-Yeon Kim[†], John Dolbow[†], and Eliot Fried[⋆]

[†] *Department of Civil and Environmental Engineering*
Duke University
Durham, NC 27708-0287

[⋆] *Department of Mechanical and Aerospace Engineering*
Washington University in St. Louis
St Louis, MO 63130-4899

Abstract

This work concerns the development of a finite-element method for discretizing a recent second-gradient theory for the flow of incompressible fluids. The new theory gives rise to a flow equation involving higher-order gradients of the velocity field and introduces an accompanying length scale and boundary conditions. Finite-element methods based on similar equations involving fourth-order differential operators typically rely on C^1-continuous basis functions or a mixed approach, both of which entail certain implementational difficulties. Here, we examine the adaptation of a relatively inexpensive, nonconforming method based on C^0-continuous basis functions. We first develop the variational form of the method and establish consistency. The method weakly enforces continuity of the vorticity, traction, and hypertraction across interelement boundaries. Stabilization is achieved via Nitsche's method. Further, pressure stabilization scales with the higher-order moduli, so that a classical formulation is recovered as a particular limit. The numerical method is verified for the problem of steady, plane Poiseuille flow. We then provide several numerical examples illustrating the robustness of the method and contrasting the predictions to those provided by classical Navier–Stokes theory.

Key words: finite-element, nonconforming, incompressible, fluid, second-gradient
PACS: 47.11.Fg, 47.11.-j, 47.85.Dh

1 Introduction

Increasingly, continuum formulations are being explored as a means to capture phenomena at smaller and smaller length scales. An essential question con-

cerns the proper strategy for extending classical theories to capture behavior that is scale dependent. While tremendous theoretical progress has been made along these lines over the past decade, the development of robust numerical methods has lagged behind. This work concerns a new finite-element method for discretizing a theory of incompressible fluid flow that incorporates length scale effects through the introduction of higher-order gradients of the velocity field. If successful in accurately representing fluid flow at small length scales, such an approach might serve as an attractive and efficient complement to methods based on molecular dynamics or atomistics.

The origins of the second-gradient theory of fluid flow can be traced back to Gurtin [1], who developed general balance equations and associated boundary conditions for a "second-grade material" using a nonstandard form of the principle of virtual power. Gurtin's work generalizes the early results provided by Toupin [2,3], who developed analogous conditions for an elastic body whose strain energy depends on first and second gradients of the deformation. The main contribution of Gurtin's work is that it is independent of constitutive assumptions. As such, it is equally applicable to fluids as solids. Fried and Gurtin [4] recently adapted this framework to develop a theory of fluid flow at small length scales. Subsequently, Fried and Gurtin [5] established a connection to the Lagrangian averaged Navier–Stokes-α model for turbulent flow. Aside from an extension of the Navier–Stokes equation involving higher-order gradients of the velocity field and involving an accompanying length scale, this framework provides consistent boundary conditions on free and fixed boundaries. The free boundary conditions involve the curvature of the free surface; among the conditions for a fixed boundary are generalized adherence and slip conditions, each of which involves a material length scale.

Our current interest is focused on examining further the predictions that this second-gradient theory for fluid flow provides. Accordingly, we discuss an advanced numerical method that is based on this new, higher-order continuum theory. The challenges include properly incorporating the higher-order velocity gradients and stabilizing the pressure field. The flow equation arising from the second-gradient theory involves fourth-order partial derivatives. Hence, a standard Galerkin approximation requires C^1-continuous basis functions such that both the velocity field and its first derivatives are continuous. Examples include functions based on Hermite polynomials. While relatively simple to construct on uniform meshes, unstructured meshes present difficulties and certain partitions are not permissible with isoparametric versions of Hermite elements; cf., e.g., Petera and Pittman [6]. Further, additional care is required to impose boundary conditions for a theory stemming from a (classically) second-order problem using elements designed for fourth-order problems. Mixed finite-element methods present a relatively expensive alternative, requiring separate approximations for primary and secondary fields; cf., e.g., Fortin and Brezzi [7].

To overcome some of the drawbacks of these traditional methods, we adapt the continuous/discontinuous Galerkin (C/DG) method proposed by Engel et al. [8]. This is essentially a nonconforming method—as the basis functions, while continuous, do not lie in the proper space for a strict Galerkin method. Continuity requirements for the derivatives are weakly satisfied by borrowing concepts from discontinuous Galerkin methods, in particular by extending the variational equation to include stabilization terms on interelement boundaries. Engel et al. [8] successfully applied the method to solve problems involving fourth-order elliptic operators arising from theories for thin beams and plates and strain gradient elasticity. Here, we develop a comparable formulation for a gradient theory for the flow of incompressible fluids.

The outline of this paper is as follows. In the next section, we introduce general balance equations and the boundary conditions developed by Fried and Gurtin [5]. Section 3 describes the weak formulation for the newly developed flow equations. In section 4, we introduce the nonconforming variational formulation and discretization with finite elements for the second-gradient theory. Numerical examples investigating the performance of the method are provided in section 5. Finally a summary and concluding remarks are given in the last section.

2 Governing Equations

We work with the generalized equations for fluid flow introduced by Fried and Gurtin [5]. The theory is based on a nonstandard form of the principle of virtual power provided by Gurtin [1]. The principle of virtual power is used as a basic tool in determining the structure of the tractions and of the local force balances. Classically, the power expended within an arbitrary control volume R in the region of space occupied by the deformed body has the simple form

$$\mathcal{W}_{\text{int}}(R) = \int_R \mathbf{T} \cdot \operatorname{grad} \mathbf{v} \, \mathrm{d}v = \int_R T_{ij} v_{i,j} \, \mathrm{d}v \tag{1}$$

with $\mathbf{T}$ the Cauchy stress and $\mathbf{T} \cdot \operatorname{grad} \mathbf{v}$ the stress power. Fried and Gurtin [5] (see also Fried and Gurtin [4]) generalize the classical theory by including, in the internal power, a term linear in the vorticity gradient $\operatorname{grad} \boldsymbol{\omega} = \operatorname{grad} \operatorname{curl} \mathbf{v}$. Specifically, a second-order tensor-valued *hyperstress* $\mathbf{G}$ is introduced via an internal power expenditure of the form $\mathbf{G} \cdot \operatorname{grad} \boldsymbol{\omega}$. The internal power expended within R then becomes

$$\mathcal{W}_{\text{int}}(R) = \int_R (\mathbf{T} \cdot \operatorname{grad} \mathbf{v} + \mathbf{G} \cdot \operatorname{grad} \boldsymbol{\omega}) \, \mathrm{d}v = \int_R (T_{ij} v_{i,j} + G_{ij} \omega_{i,j}) \, \mathrm{d}v. \tag{2}$$

In conjunction with the internal power expenditure (2), Fried and Gurtin [5] introduce a corresponding external power expenditure

$$\mathcal{W}_{\rm ext}(R) = \int\limits_{\mathcal{S}} \left(\mathbf{t}_{\mathcal{S}} \cdot \mathbf{v} + \mathbf{m}_{\mathcal{S}} \cdot \frac{\partial \mathbf{v}}{\partial n} \right) {\rm d}a + \int\limits_{R} \mathbf{b} \cdot \mathbf{v} \, {\rm d}v, \tag{3}$$

in which $\mathbf{t}_{\mathcal{S}}$ and $\mathbf{m}_{\mathcal{S}}$ represent tractions on the bounding surface $\mathcal{S} = \partial R$ of R, while $\mathbf{b}$ *represents the net inertial and noninertial body force* acting within the body. Here the term

$$\mathbf{m}_{\mathcal{S}} \cdot \frac{\partial \mathbf{v}}{\partial n} \, ,$$

which is not present in classical theories, is needed to balance the effects of the internal-power term $\mathbf{G} \cdot \cdot \, {\rm grad}\, \boldsymbol{\omega}$, which involves the second gradient of $\mathbf{v}$.

The principle of virtual power replaces $\mathbf{v}$ by $\tilde{\mathbf{v}}$ and $\boldsymbol{\omega}$ by ${\rm curl}\, \tilde{\mathbf{v}}$ and is based on the requirement that

$$\mathcal{W}_{\rm ext}(R, \tilde{\mathbf{v}}) = \mathcal{W}_{\rm int}(R, \tilde{\mathbf{v}}) \tag{4}$$

for all control volumes R and any choice of the virtual velocity field $\tilde{\mathbf{v}}$. Consequences of the virtual power principle and the requirement that the internal power expenditure be frame-indifferent are that:

(i) The classical macroscopic balance $\rho \dot{\mathbf{v}} = {\rm div}\, \mathbf{T}$ must be replaced by the balance

$$\rho \dot{\mathbf{v}} = {\rm div}\, \mathbf{T} + {\rm curl}\, {\rm div}\, \mathbf{G}, \tag{5}$$

with $\mathbf{T}$ symmetric as in the classical theory.

(ii) Cauchy's classical condition $\mathbf{t}_{\mathcal{S}} = \mathbf{T}\mathbf{n}$ for the traction across a surface $\mathcal{S}$ with unit normal $\mathbf{n}$ must be replaced by the conditions

$$\left.\begin{aligned} \mathbf{t}_{\mathcal{S}} &= \mathbf{T}\mathbf{n} + {\rm div}_{\mathcal{S}}(\mathbf{G}\mathbf{n}\times) + \mathbf{n} \times ({\rm div}\, \mathbf{G} - 2K\mathbf{G}\mathbf{n}), \\ \mathbf{m}_{\mathcal{S}} &= \mathbf{n} \times \mathbf{G}\mathbf{n}, \end{aligned} \right\} \tag{6}$$

in which ${\rm div}_{\mathcal{S}}$ is the divergence operator on $\mathcal{S}$ and $K = -\frac{1}{2}{\rm div}_{\mathcal{S}}\mathbf{n}$ is the mean curvature of $\mathcal{S}$.

When supplemented by constitutive equations for the stress and hyperstress, the balance (5) yields a flow equation. Restricting attention to incompressible fluids, we invoke the standard decomposition

$$\mathbf{T} = \mathbf{S} - p\mathbf{1}, \qquad {\rm tr}\, \mathbf{S} = 0, \tag{7}$$

of the stress into a traceless extra stress $\mathbf{S}$ and a powerless pressure p and take the extra stress to be of the form

$$\mathbf{S} = 2\mu \mathbf{D}, \qquad \mu > 0, \tag{8}$$

where $\mathbf{D} = \frac{1}{2}(\operatorname{grad}\mathbf{v} + (\operatorname{grad}\mathbf{v})^\top)$ is the stretch-rate.[1] Further, we take the hyperstress to be of the simple linear form

$$\mathbf{G} = \zeta \operatorname{grad}\boldsymbol{\omega} + \xi(\operatorname{grad}\boldsymbol{\omega})^\top, \tag{9}$$

with $\zeta > 0$ and $-\zeta \leq \xi \leq \zeta$ to ensure non-negative dissipation.

Using (7)–(9) in (5) and assuming that the moduli μ, ζ, and ξ are constant, we arrive at the flow equation

$$\rho\dot{\mathbf{v}} = -\operatorname{grad} p + \mu\Delta\mathbf{v} - \zeta\Delta\Delta\mathbf{v}, \tag{10}$$

which, in components, has the equivalent form $\rho\dot{v}_i = -p_{,i} + \mu v_{i,jj} - \zeta v_{i,jjkk}$. In this equation $\mathbf{v}$ is subject to the incompressibility constraint

$$\operatorname{div}\mathbf{v} = 0, \tag{11}$$

$\dot{\mathbf{v}}$ (often written as $\mathrm{D}\mathbf{v}/\mathrm{D}t$) is the material time derivative of $\mathbf{v}$, p is the pressure, and Δ is the Laplace operator.

Returning to the general flow equation (10), we may identify the characteristic length scale

$$L = \sqrt{\frac{\zeta}{\mu}}. \tag{12}$$

Fried and Gurtin [4] refer to L as the gradient length and we use that terminology here as well.

In addition to the flow equation, the theory also provides boundary conditions. In particular, the classical no-slip boundary boundary condition is replaced by the generalized adherency conditions

$$\mathbf{v} = \mathbf{0} \qquad \text{and} \qquad \mathbf{m}_s = -\mu l\boldsymbol{\omega}\times\mathbf{n}, \tag{13}$$

in which the constitutive modulus $l \geq 0$, the adherence length, measures the strength of the fluid's adherence to the boundary. Alternatively, the theory provides conditions at solid boundaries with slip and conditions at free surfaces, each of which involves the introduction of an additional constitutive parameter.

3 Variational Formulation

Because the general flow equation (5) and boundary conditions (6) follow from the application of the principle of virtual power, it is fairly straightforward

[1] We note that Fried and Gurtin [5] include a term proportional to the corotational rate of $\mathbf{D}$ in the extra stress. That term is neglected here.

to derive a variational formulation of the flow equation and the boundary conditions (13). Here rather than using an arbitrary control volume R, we work with the region B occupied by the body at a fixed time t.

We consider *boundary conditions* in which a portion $\mathcal{S}_{\text{free}}$ of ∂B is free and the remainder $\mathcal{S}_{\text{fxd}}$ is fixed:

$$\left.\begin{aligned} \left.\begin{aligned} \mathbf{T}\mathbf{n} + \operatorname{div}_{\mathcal{S}}(\mathbf{G}\mathbf{n}\times) + \mathbf{n}\times\operatorname{div}\mathbf{G} = \sigma K\mathbf{n} \\ \text{and} \quad \mathbf{n}\times\mathbf{G}\mathbf{n} = \mathbf{0} \end{aligned}\right\} \quad \text{on} \quad \mathcal{S}_{\text{free}}, \\ \mathbf{v} = \mathbf{0} \quad \text{and} \quad \mathbf{n}\times\mathbf{G}\mathbf{n} = -\mu l\boldsymbol{\omega}\times\mathbf{n} \quad \text{on} \quad \mathcal{S}_{\text{fxd}}; \end{aligned}\right\} \tag{14}$$

cf. (13). Here, σ denotes the surface tension.

We refer to an arbitrary virtual field $\tilde{\mathbf{v}}$ as *kinematically admissible* if

$$\tilde{\mathbf{v}} = \mathbf{0} \text{ on } \mathcal{S}_{\text{fxd}}. \tag{15}$$

Given such a field, we consider the virtual-power balance (4) applied with $R = B$, neglecting (noninertial) body forces, and with the replacements indicated by

$$\mathbf{t}_{\mathcal{S}} \to \sigma K\mathbf{n} \text{ and } \mathbf{m}_{\mathcal{S}} \to \mathbf{0} \text{ on } \mathcal{S}_{\text{free}}, \qquad \mathbf{m}_{\mathcal{S}} \to -\mu l\boldsymbol{\omega}\times\mathbf{n} \text{ on } \mathcal{S}_{\text{fxd}}. \tag{16}$$

We write $\mathcal{V}$ and $\mathcal{P}$ for the spaces of admissible velocity and pressure fields, respectively. The two-field variational form reads: find $(\mathbf{v}, p) \in \mathcal{V}\times\mathcal{P}$ such that

$$T(\mathbf{v}, p, \tilde{\mathbf{v}}, \tilde{p}) = \ell(\tilde{\mathbf{v}}) \tag{17}$$

for all $(\tilde{\mathbf{v}}, \tilde{p}) \in \mathcal{V}\times\mathcal{P}$, where

$$\begin{aligned} T(\mathbf{v}, p, \tilde{\mathbf{v}}, \tilde{p}) = &\int_B (\mathbf{S}\,\vdots\,\operatorname{grad}\tilde{\mathbf{v}} + \mathbf{G}\,\vdots\,\operatorname{grad}\operatorname{curl}\tilde{\mathbf{v}})\,\mathrm{d}v + \int_{\mathcal{S}_{\text{fxd}}} (\mu l\boldsymbol{\omega}\times\mathbf{n})\cdot\frac{\partial\tilde{\mathbf{v}}}{\partial n}\,\mathrm{d}a \\ &- \int_B p\operatorname{div}\tilde{\mathbf{v}}\,\mathrm{d}v - \int_B \tilde{p}\operatorname{div}\mathbf{v}\,\mathrm{d}v - \int_B \rho\dot{\mathbf{v}}\cdot\tilde{\mathbf{v}}\,\mathrm{d}v, \end{aligned} \tag{18}$$

and

$$\ell(\tilde{\mathbf{v}}) = \int_{\mathcal{S}_{\text{free}}} \sigma K\mathbf{n}\cdot\tilde{\mathbf{v}}\,\mathrm{d}a. \tag{19}$$

To obtain correspondence with the particular flow equation (10), $\mathbf{S}$ and $\mathbf{G}$ are given by (8) and (9), respectively.

4 Discretization of the Second Gradient Theory

In this section, we introduce our numerical formulation for the second-gradient theory. Our work is based on the nonconforming method proposed by Engel et al. [8]. In this approach, the basis functions are C^0-continuous—so that their first and higher-order derivatives are discontinuous. Continuity of the first and higher-order derivatives is weakly enforced by adding weighted residual terms to the variational equation on element boundaries and invoking stabilization techniques. The number of unknowns per element arising for this method is considerably fewer than for alternatives based on traditional strategies such as C^1-continuous basis functions.

The spaces of admissible velocity and pressure fields are $\mathcal{V} \subset H^2(B)$ and $\mathcal{P} \subset H^0(B)$, where $H^m(B)$ denotes the classical Sobolev space of order m. We use a nonconforming Galerkin method to approximate the solution to (17), and we state the weak form of the variational problem in terms of finite-dimensional spaces $\mathcal{V}^h \subset H^1(B)$ and $\mathcal{P}^h \subset \mathcal{P}$.

To construct the bases, we consider a regular finite-element partition $\mathcal{Q}^h = \cup_{e=1}^{M} \mathcal{Q}_e$, with $\mathcal{Q}^h \approx B$ and M the total number of elements in the mesh. We choose approximation functions which are continuous on the entire domain but discontinuous in first and higher-order derivatives across element boundaries. Further, we consider element interiors $\tilde{\mathcal{Q}}$ defined via

$$\tilde{\mathcal{Q}} = \bigcup_{e=1}^{M} \mathcal{Q}_e. \tag{20}$$

The union $\tilde{\Gamma}$ of interior boundaries is expressed as

$$\tilde{\Gamma} = \bigcup_{i=1}^{N_i} \Gamma_i, \tag{21}$$

where N_i denotes the number of element *interior* boundaries. In two dimensions, these refer only to those element edges that are shared by two spatially adjacent elements, and do not include edges along the physical boundary ∂B. Given a field f on B, the jump $[\![f]\!]$ of f across the interior boundary is defined as

$$[\![f]\!] = f^+ - f^-. \tag{22}$$

where

$$f^{\pm} = \lim_{\epsilon \to 0} f(\mathbf{x} \mp \epsilon \mathbf{n}) \tag{23}$$

and $\mathbf{n}$ is any of the two unit normals to the interior boundary and $\epsilon > 0$. The jump operator is graphically described in Figure 1. The average $\langle\!\langle f \rangle\!\rangle$ of f

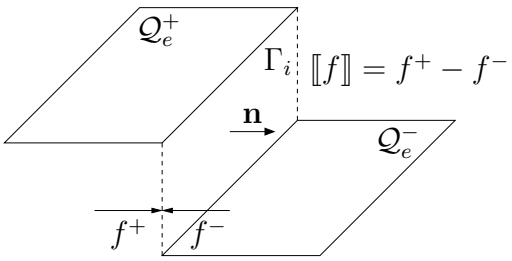

Fig. 1. Graphical description of jump operator

across the interior boundary is defined as

$$\langle\!\langle f \rangle\!\rangle = \frac{1}{2}(f^+ + f^-). \tag{24}$$

From the definitions of the jump and average operators, we have the useful identity

$$[\![fg]\!] = [\![f]\!]\langle\!\langle g \rangle\!\rangle + \langle\!\langle f \rangle\!\rangle [\![g]\!]. \tag{25}$$

The method we propose to approximate the solution to flow problems arising from the second-gradient theory can then be stated as: find $(\mathbf{v}^h, p^h) \in \mathcal{V}^h \times \mathcal{P}^h$ such that

$$T_{cd}(\mathbf{v}^h, p^h, \tilde{\mathbf{v}}^h, \tilde{p}^h) = \ell_{cd}(\tilde{\mathbf{v}}^h), \quad \forall\ (\tilde{\mathbf{v}}^h, \tilde{p}^h) \in \mathcal{V}^h \times \mathcal{P}^h, \tag{26}$$

where the bilinear form T_{cd} is defined via

$$\begin{aligned} T_{cd}(\mathbf{v}^h, p^h, \tilde{\mathbf{v}}^h, \tilde{p}^h) = &\int_{\tilde{\mathcal{Q}}} (\mathbf{S}^h : \operatorname{grad} \tilde{\mathbf{v}}^h + \mathbf{G}^h : \operatorname{grad}\operatorname{curl} \tilde{\mathbf{v}}^h)\, \mathrm{d}v - \int_{\tilde{\Gamma}_{\text{int}}} \langle\!\langle \tilde{\mathbf{G}}^h \mathbf{n} \rangle\!\rangle \cdot [\![\operatorname{curl} \mathbf{v}^h]\!]\, \mathrm{d}a \\ &- \int_{\tilde{\Gamma}} [\![\operatorname{curl} \tilde{\mathbf{v}}^h]\!] \cdot \langle\!\langle \mathbf{G}^h \mathbf{n} \rangle\!\rangle\, \mathrm{d}a + \tau_v \int_{\tilde{\Gamma}} [\![\operatorname{curl} \tilde{\mathbf{v}}^h]\!] \cdot [\![\operatorname{curl} \mathbf{v}^h]\!]\, \mathrm{d}a \\ &- \int_{\tilde{\mathcal{Q}}} p^h \operatorname{div} \tilde{\mathbf{v}}^h\, \mathrm{d}v - \int_{\tilde{\mathcal{Q}}} \tilde{p}^h \operatorname{div} \mathbf{v}^h\, \mathrm{d}v - \int_{\tilde{\mathcal{Q}}} \rho \dot{\mathbf{v}}^h \cdot \tilde{\mathbf{v}}^h\, \mathrm{d}v \end{aligned} \tag{27}$$

and the linear form ℓ_{cd} is defined via

$$\ell_{cd}(\tilde{\mathbf{v}}^h) = \int_{\mathcal{S}_{\text{free}}} \sigma K \mathbf{n} \cdot \tilde{\mathbf{v}}^h\, \mathrm{d}a - \int_{\mathcal{S}_{\text{fxd}}} (\mu l \boldsymbol{\omega} \times \mathbf{n}) \cdot \frac{\partial \tilde{\mathbf{v}}^h}{\partial n}\, \mathrm{d}a. \tag{28}$$

In (27), τ_v denotes the velocity stabilization parameter for the interelement boundaries. The basic structure of this stabilized approach follows from Nitsche's method [10] for enforcing constraints on interfaces.

Many of the jump terms appearing in (27) stem from the divergence theorem as applied to volume integrals over individual elements (see the following proof

of consistency). In particular, surface integrals involving normal flux quantities (such as $\mathbf{T}\mathbf{n}_e$ or $\mathbf{G}\mathbf{n}_e$) arise over the boundary of each element $\mathcal{Q}_e$, where $\mathbf{n}_e$ denotes the unit outward normal to $\mathcal{Q}_e$. Since adjacent elements possess equal and opposite normal vectors along common interior boundaries, the choice of positive normal (and thus positive side) is arbitrary for any given pair. However, for consistency, it is important that once a positive side is identified on a given element interior, it is identified as such for each of the jump terms appearing in (27).

4.1 Consistency

The consistency of the method is derived through successive application of the divergence theorem to (26). Using the equality (25), we derive

$$\begin{aligned}\int_{\tilde{\mathcal{Q}}} \mathbf{T}^h : \operatorname{grad} \tilde{\mathbf{v}}^h \,\mathrm{d}v &= -\int_{\tilde{\mathcal{Q}}} \operatorname{div} \mathbf{T}^h \cdot \tilde{\mathbf{v}}^h \,\mathrm{d}v + \int_{\mathcal{S}} \mathbf{T}^h \mathbf{n} \cdot \tilde{\mathbf{v}}^h \,\mathrm{d}a + \int_{\tilde{\Gamma}} [\![\mathbf{T}^h \mathbf{n} \cdot \tilde{\mathbf{v}}^h]\!] \,\mathrm{d}a \\ &= -\int_{\tilde{\mathcal{Q}}} \operatorname{div} \mathbf{T}^h \cdot \tilde{\mathbf{v}}^h \,\mathrm{d}v + \int_{\mathcal{S}} \mathbf{T}^h \mathbf{n} \cdot \tilde{\mathbf{v}}^h \,\mathrm{d}a \\ &\qquad + \int_{\tilde{\Gamma}} \left([\![\mathbf{T}^h \mathbf{n}]\!] \cdot \langle\!\langle \tilde{\mathbf{v}}^h \rangle\!\rangle + \langle\!\langle \mathbf{T}^h \mathbf{n} \rangle\!\rangle \cdot [\![\tilde{\mathbf{v}}^h]\!] \right) \mathrm{d}a.\end{aligned}$$

Similarly, the divergence theorem applied twice yields

$$\begin{aligned}\int_{\tilde{\mathcal{Q}}} \mathbf{G}^h : \operatorname{grad} \operatorname{curl} \tilde{\mathbf{v}}^h \,\mathrm{d}v &= -\int_{\tilde{\mathcal{Q}}} (\operatorname{div} \mathbf{G}^h) \cdot (\operatorname{curl} \tilde{\mathbf{v}}^h) \,\mathrm{d}v + \int_{\mathcal{S}} \mathbf{G}^h \mathbf{n} \cdot \operatorname{curl} \tilde{\mathbf{v}}^h \,\mathrm{d}a \\ &\qquad + \int_{\tilde{\Gamma}} [\![\mathbf{G}^h \mathbf{n} \cdot \operatorname{curl} \tilde{\mathbf{v}}^h]\!] \,\mathrm{d}a \\ &= -\int_{\tilde{\mathcal{Q}}} (\operatorname{curl} \operatorname{div} \mathbf{G}^h) \cdot \tilde{\mathbf{v}}^h \,\mathrm{d}v + \int_{\mathcal{S}} (\mathbf{G}^h \mathbf{n} \cdot \operatorname{curl} \tilde{\mathbf{v}}^h + (\mathbf{n} \times \operatorname{div} \mathbf{G}^h) \cdot \tilde{\mathbf{v}}^h) \,\mathrm{d}a \\ &\qquad + \int_{\tilde{\Gamma}} \left([\![\mathbf{G}^h \mathbf{n} \cdot \operatorname{curl} \tilde{\mathbf{v}}^h]\!] + [\![(\mathbf{n} \times \operatorname{div} \mathbf{G}^h) \cdot \tilde{\mathbf{v}}^h]\!] \right) \mathrm{d}a \\ &= -\int_{\tilde{\mathcal{Q}}} (\operatorname{curl} \operatorname{div} \mathbf{G}^h) \cdot \tilde{\mathbf{v}}^h \,\mathrm{d}v + \int_{\mathcal{S}} (\mathbf{G}^h \mathbf{n} \cdot \operatorname{curl} \tilde{\mathbf{v}}^h + (\mathbf{n} \times \operatorname{div} \mathbf{G}^h) \cdot \tilde{\mathbf{v}}^h) \,\mathrm{d}a \\ &\qquad + \int_{\tilde{\Gamma}} \left([\![\mathbf{G}^h \mathbf{n}]\!] \cdot \langle\!\langle \operatorname{curl} \tilde{\mathbf{v}}^h \rangle\!\rangle + \langle\!\langle \mathbf{G}^h \mathbf{n} \rangle\!\rangle \cdot [\![\operatorname{curl} \tilde{\mathbf{v}}^h]\!] \right) \mathrm{d}a \\ &\qquad\qquad + \int_{\tilde{\Gamma}} \left([\![\mathbf{n} \times \operatorname{div} \mathbf{G}^h]\!] \cdot \langle\!\langle \tilde{\mathbf{v}}^h \rangle\!\rangle + \langle\!\langle (\mathbf{n} \times \operatorname{div} \mathbf{G}^h) \rangle\!\rangle \cdot [\![\tilde{\mathbf{v}}^h]\!] \right) \mathrm{d}a.\end{aligned}$$

Since $\tilde{\mathbf{v}}^h$ is continuous on the interelement boundary $\tilde{\Gamma}$, we have $[\![\tilde{\mathbf{v}}^h]\!] = \mathbf{0}$, yielding

$$\int_{\tilde{\mathcal{Q}}} \mathbf{T}^h : \operatorname{grad} \tilde{\mathbf{v}}^h \, \mathrm{d}v = -\int_{\tilde{\mathcal{Q}}} \operatorname{div} \mathbf{T}^h \cdot \tilde{\mathbf{v}}^h \, \mathrm{d}v + \int_{\mathcal{S}} \mathbf{T}^h \mathbf{n} \cdot \tilde{\mathbf{v}}^h \, \mathrm{d}a + \int_{\tilde{\Gamma}} [\![\mathbf{T}^h \mathbf{n}]\!] \cdot \langle\!\langle \tilde{\mathbf{v}}^h \rangle\!\rangle \, \mathrm{d}a \quad (29)$$

and

$$\begin{aligned} \int_{\tilde{\mathcal{Q}}} \mathbf{G}^h : \operatorname{grad} \operatorname{curl} \tilde{\mathbf{v}}^h \, \mathrm{d}v = &-\int_{\tilde{\mathcal{Q}}} (\operatorname{curl} \operatorname{div} \mathbf{G}^h) \cdot \tilde{\mathbf{v}}^h \, \mathrm{d}v \\ &+ \int_{\mathcal{S}} (\mathbf{G}^h \mathbf{n} \cdot \operatorname{curl} \tilde{\mathbf{v}}^h + (\mathbf{n} \times \operatorname{div} \mathbf{G}^h) \cdot \tilde{\mathbf{v}}^h) \, \mathrm{d}a \\ &+ \int_{\tilde{\Gamma}} \Big([\![\mathbf{G}^h \mathbf{n}]\!] \cdot \langle\!\langle \operatorname{curl} \tilde{\mathbf{v}}^h \rangle\!\rangle + \langle\!\langle \mathbf{G}^h \mathbf{n} \rangle\!\rangle \cdot [\![\operatorname{curl} \tilde{\mathbf{v}}^h]\!] \Big) \, \mathrm{d}a \\ &+ \int_{\tilde{\Gamma}} [\![\mathbf{n} \times \operatorname{div} \mathbf{G}^h]\!] \cdot \langle\!\langle \tilde{\mathbf{v}}^h \rangle\!\rangle \, \mathrm{d}a. \end{aligned} \quad (30)$$

Here, we take advantage of the equality

$$\int_{\mathcal{S}} \mathbf{G}^h \mathbf{n} \cdot \operatorname{curl} \tilde{\mathbf{v}}^h \, \mathrm{d}a = \int_{\mathcal{S}} \left((\operatorname{div}_{\mathcal{S}} (\mathbf{G}^h \mathbf{n} \times) - 2K \mathbf{n} \times \mathbf{G}^h \mathbf{n}) \cdot \tilde{\mathbf{v}}^h + (\mathbf{n} \times \mathbf{G}^h \mathbf{n}) \cdot \frac{\partial \tilde{\mathbf{v}}^h}{\partial n} \right) \mathrm{d}a, \quad (31)$$

A detailed derivation of this equality is provided by Fried and Gurtin [5].

The consistency of the method then follows upon substituting the results (29), (30), and (31), into (27), viz.

$$\begin{aligned} 0 = \; & T_{cd}(\mathbf{v}^h, p^h, \tilde{\mathbf{v}}^h, \tilde{p}^h) - \ell_{cd}(\tilde{\mathbf{v}}^h) \\ = \; & \int_{\tilde{\mathcal{Q}}} (\operatorname{curl} \operatorname{div} \mathbf{G}^h + \operatorname{div} \mathbf{T}^h - \rho \dot{\mathbf{v}}^h) \cdot \tilde{\mathbf{v}}^h \, \mathrm{d}v - \int_{\tilde{\Gamma}} \langle\!\langle \tilde{\mathbf{G}}^h \mathbf{n} \rangle\!\rangle \cdot [\![\operatorname{curl} \mathbf{v}^h]\!] \, \mathrm{d}a \\ & + \int_{\tilde{\Gamma}} [\![\mathbf{T}^h \mathbf{n} + \mathbf{n} \times \operatorname{div} \mathbf{G}^h + \operatorname{div}_{\mathcal{S}} (\mathbf{G}^h \mathbf{n} \times) - 2K \mathbf{n} \times \mathbf{G}^h \mathbf{n}]\!] \cdot \langle\!\langle \tilde{\mathbf{v}}^h \rangle\!\rangle \, \mathrm{d}a \\ & + \int_{\tilde{\Gamma}} [\![\mathbf{n} \times \mathbf{G}^h \mathbf{n}]\!] \cdot \left\langle\!\!\left\langle \frac{\partial \tilde{\mathbf{v}}^h}{\partial n} \right\rangle\!\!\right\rangle \mathrm{d}a \\ & + \int_{\mathcal{S}_{\text{free}}} (\mathbf{T}^h \mathbf{n} + \mathbf{n} \times \operatorname{div} \mathbf{G}^h + \operatorname{div}_{\mathcal{S}} (\mathbf{G}^h \mathbf{n} \times) - 2K \mathbf{n} \times \mathbf{G}^h \mathbf{n} - \sigma K \mathbf{n}) \cdot \tilde{\mathbf{v}}^h \, \mathrm{d}a \\ & + \int_{\mathcal{S}_{\text{free}}} (\mathbf{n} \times \mathbf{G}^h \mathbf{n}) \cdot \frac{\partial \tilde{\mathbf{v}}^h}{\partial n} \, \mathrm{d}a + \int_{\mathcal{S}_{\text{fxd}}} (\mathbf{n} \times \mathbf{G}^h \mathbf{n} - \mu l \boldsymbol{\omega} \times \mathbf{n}) \cdot \frac{\partial \tilde{\mathbf{v}}^h}{\partial n} \, \mathrm{d}a \\ & + \tau_v \int_{\tilde{\Gamma}} [\![\operatorname{curl} \tilde{\mathbf{v}}^h]\!] \cdot [\![\operatorname{curl} \mathbf{v}^h]\!] \, \mathrm{d}a. \end{aligned} \quad (32)$$

From (32) we deduce the second gradient equations

$$\operatorname{div}\mathbf{T}^h + \operatorname{curl}\operatorname{div}\mathbf{G}^h = \rho\dot{\mathbf{v}}^h \quad \text{in} \quad \tilde{\mathcal{Q}}, \tag{33}$$

$$\left.\begin{aligned} &\left.\begin{aligned} &\mathbf{T}^h\mathbf{n} + \mathbf{n}\times\operatorname{div}\mathbf{G}^h + \operatorname{div}_{\mathcal{S}}(\mathbf{G}^h\mathbf{n}\times) - 2K\mathbf{n}\times\mathbf{G}^h\mathbf{n} = \sigma K\mathbf{n} \\ &\text{and} \quad \mathbf{n}\times\mathbf{G}^h\mathbf{n} = \mathbf{0} \end{aligned}\right\} \quad \text{on} \quad \mathcal{S}_{\text{free}}, \\ &\mathbf{n}\times\mathbf{G}^h\mathbf{n} = -\mu l\boldsymbol{\omega}\times\mathbf{n} \quad \text{on} \quad \mathcal{S}_{\text{fxd}}, \end{aligned}\right\} \tag{34}$$

and the jump conditions

$$\left.\begin{aligned} [\![\operatorname{curl}\mathbf{v}^h]\!] &= \mathbf{0}, \\ [\![\mathbf{T}^h\mathbf{n} + \mathbf{n}\times\operatorname{div}\mathbf{G}^h + \operatorname{div}_{\mathcal{S}}(\mathbf{G}^h\mathbf{n}\times) - 2K\mathbf{n}\times\mathbf{G}^h\mathbf{n}]\!] &= \mathbf{0}, \\ [\![\mathbf{n}\times\mathbf{G}^h\mathbf{n}]\!] &= \mathbf{0}, \end{aligned}\right\} \quad \text{on} \quad \tilde{\Gamma}. \tag{35}$$

While (33) enforces the flow equation on the element interiors, (34) enforces the boundary conditions on free and fixed surfaces of the flow domain, $(35)_1$ ensures the continuity of the first derivatives across the interelement boundaries, and $(35)_{2,3}$ ensure the continuity of the tractions across the interelement boundaries. On replacing $\mathbf{v}$ and p in (26) by $\mathbf{v}^h$ and p^h, we obtain the Galerkin orthogonality condition

$$T_{cd}(\mathbf{e}_v, \mathbf{e}_p, \tilde{\mathbf{v}}^h, \tilde{p}^h) = 0 \quad \forall\ (\tilde{\mathbf{v}}^h, \tilde{p}^h) \in \mathcal{V}^h \times \mathcal{P}^h, \tag{36}$$

where $\mathbf{e}_v = \mathbf{v}^h - \mathbf{v}$ and $\mathbf{e}_p = p^h - p$ are the errors for the velocity and pressure fields, respectively.

4.2 Element Choice and Additional Pressure Stabilization

We restrict attention to problems for which the inertial terms appearing in (27) can be neglected. Extensions to time-dependent flows and the nonlinearities associated with the material derivative of the velocity field for the second gradient theory are left for a future work.

We will base our formulation on one that is stable for the classical theory, namely: four-node isoparametric quadrilateral elements with piecewise-quadratic basis functions for the velocity field and linear (discontinuous) basis functions for the pressure field. Three-dimensional generalizations of these elements are readily available and widely used in practice.

To begin, we introduce the space

$$P^j(\mathcal{Q}_e) = \{\mathbf{v} : \mathbf{v} \text{ is a polynomial of degree} \leq j \text{ on } \mathcal{Q}_e\} \tag{37}$$

of complete polynomials over element $\mathcal{Q}_e$. Using N to denote the number of nodes in the mesh, we then write

$$\{\phi_I\} = \{\phi_I \in C^0(\mathcal{Q}^h) : \phi_I|\mathcal{Q}_e \in P^2(\mathcal{Q}_e)\}, \quad I = 1 \ldots N, \tag{38}$$

for the set of quadratic Lagrangian isoparametric functions. The approximation to the velocity field is then given by

$$\mathbf{v}^h(\mathbf{x}) = \sum_{I=1}^{N} \phi_I(\boldsymbol{\xi}(\mathbf{x}))\mathbf{v}_I, \tag{39}$$

where $\mathbf{v}_I$ is the nodal value at node I and $\boldsymbol{\xi}$ the coordinates in a reference element.

For the pressure field, we introduce the set

$$\{M_I\} = \{M_I \in H^0(\mathcal{Q}^h) : M_I|\mathcal{Q}_e \in P^1(\mathcal{Q}_e)\}, \quad I = 1 \ldots M, \tag{40}$$

of linear element-based (discontinuous) shape functions. The approximation to the pressure field p can then be written as

$$p^h(\mathbf{x}) = \sum_{I} M_I(\mathbf{x})p_I. \tag{41}$$

The approximations (39) and (41) over quadrilateral elements are stable for the classical problem of Stokes flow; cf., e.g., Hughes [9]. We therefore expect stability to also hold for sufficiently small gradient lengths L. However, for larger gradient lengths, we should not expect these elements to be stable. Accordingly, we investigate the use of additional pressure stabilization. In particular, we follow the approach of Hughes and Franca [11] and add terms of the form

$$-\sum_{e \in \tilde{\Gamma}} \tau_p \int_e [\![p^h]\!][\![\tilde{p}^h]\!] \, \mathrm{d}a, \tag{42}$$

to the nonconforming approximation (27), where τ_p is the pressure stability parameter. Importantly, the addition of this term does not affect the consistency proof presented earlier; indeed, this term simply enforces continuity of the pressure field between elements.

To approximate the weight functions $\tilde{\mathbf{v}}^h$ and $\tilde{p}^h$, we use expansions analogous to (39) and (41). Upon substituting these expressions into (27) (neglecting inertial terms) and invoking the arbitrariness of the weight functions, we obtain

the linear algebraic system of equations

$$\begin{bmatrix} \mathbf{K}_c + \mathbf{K}_g & \mathbf{G}_c \\ \mathbf{G}_c^\top & \mathbf{S} \end{bmatrix} \begin{bmatrix} \mathbf{d}_v \\ \mathbf{d}_p \end{bmatrix} = \begin{bmatrix} \mathbf{f}_v \\ \mathbf{f}_p \end{bmatrix}, \tag{43}$$

which can be solved to yield $\mathbf{d}_v$ and $\mathbf{d}_p$.

5 Numerical Examples

5.1 Benchmark Problem: Plane Poiseuille Flow

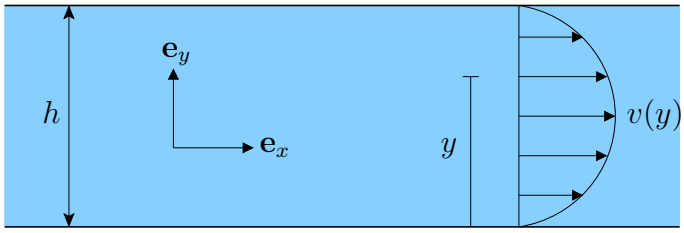

Fig. 2. Schematic of the channel for the problem of plane Poiseuille flow. The coordinates in the directions downstream and out of the plane are x and z.

We consider the problem of steady, laminar flow through an infinite, rectangular channel formed by two parallel surfaces separated by a gap h (Figure 2). Writing

$$u = \mathbf{v}\cdot\mathbf{e}_x, \quad v = \mathbf{v}\cdot\mathbf{e}_y, \tag{44}$$

for the horizontal and vertical components of the velocity field, we consider problems with solutions of the form

$$u = u(y), \quad v = 0, \tag{45}$$

as shown in Figure 2. An analytical solution to this problem for the flow equation (10) with generalized adherency conditions (13) was developed by Fried and Gurtin [4] for a theory different from that considered here. Nevertheless, the solution to the problem of plane Poiseuille flow is identical for both theories.

The pressure field is only known up to an arbitrary additive constant with gradient

$$\operatorname{grad} p = -\beta\mathbf{e}_x, \qquad \text{with} \qquad \beta = \text{constant}; \tag{46}$$

without loss of generality, we assume that $\beta > 0$. The solution for the velocity field can be decomposed into classical and generalized contributions as

$$u(y) = u_c(y) + u_g(y), \tag{47}$$

where

$$u_c(y) = \frac{\beta h^2}{2\mu}\frac{y}{h}\left(1 - \frac{y}{h}\right) \tag{48}$$

is the *classical solution* of the analogous problem for a Navier–Stokes fluid and

$$u_g(y) = -\frac{\beta h^2}{2\mu}\frac{b_l L}{h \sinh\frac{h}{L}}\left(\sinh\frac{h}{L} - \sinh\frac{y}{L} - \sinh\frac{h-y}{L}\right) \tag{49}$$

arises from higher-order terms characterized by the gradient length L. In view of the signs of L, l, and h, the constant

$$b_l = \frac{\frac{2L}{h} + \frac{l}{L}}{1 + \frac{l}{L}\tanh\frac{h}{2L}} \tag{50}$$

is a nonnegative dimensionless measure of the effective adhesion length. The specialized conditions of weak and strong adherence arise respectively from the limits setting $l \to 0$ and $l \to \infty$.

Although the solution (49) is essentially one-dimensional in nature, we use it to establish a two-dimensional boundary value problem to verify the finite-element formulation described in Section 4. The approach we follow is to prescribe boundary conditions consistent with (49) on an arbitrary, finite "computational domain" $\mathcal{Q}^h$. We then quantify the error in the numerical approximation to the velocity $\mathbf{v}$ and pressure p fields on the interior of the domain using suitable error norms. This procedure requires a-priori knowledge of the solution and is only used for verifying the numerical formulation. More general boundary conditions will be discussed subsequently.

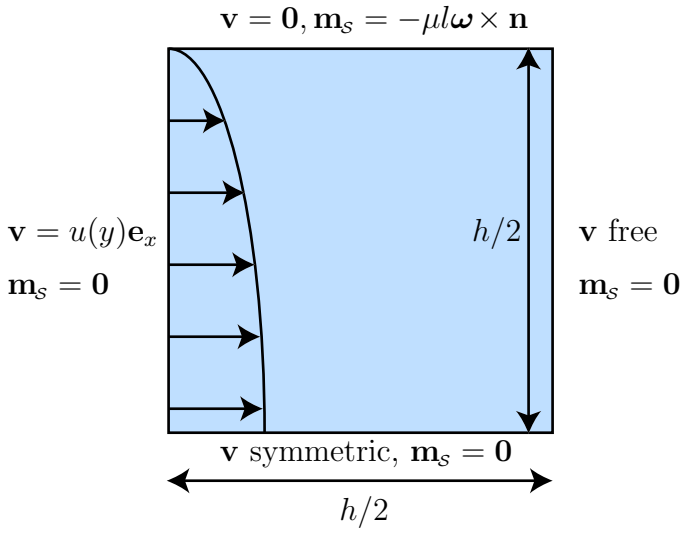

Fig. 3. Computational domain and boundary conditions for the channel flow studies.

We take advantage of the symmetry of the solution (49) about the midplane of the channel and consider a numerical domain with dimensions $[0, h/2] \times [h/2, h]$

as shown in Figure 3. On the midplane of the channel, the velocity field is constrained to be symmetric and a zero hypertraction is enforced. The top surface of the channel is considered fixed and we prescribe the generalized adherence conditions (13). It bears emphasis that while the vertical component of the velocity field is fixed to vanish on all of the boundaries of the computational domain, it is not constrained on the interior of the domain.

What remains is to designate boundary conditions on the vertical computational surfaces. Here, we choose to prescribe the velocity field only at the left (inlet) boundary according to the exact solution (49). Zero hypertractions are prescribed at the inlet and outlet.

To check convergence in the velocity field, we use the L_2-norm of the error $\mathbf{e}_v = \mathbf{v}^h - \mathbf{v}$. Since the pressure field is known only up to a constant, the appropriate norm to check convergence is the L_2-norm of the error $\mathbf{e}_p = \operatorname{grad} p^h - \operatorname{grad} p$ in the gradient of the pressure field. In the following, we report error norms that are normalized by those of the solution.

We begin by examining the limiting case of $l \to 0$, corresponding to weak adherence conditions on the channel walls. We set the gradient length L equal to $h/4$. Figure 4 provides convergence results obtained using a sequence of uniform meshes with equidistant nodal spacing $\mathrm{d}y = \mathrm{d}x$ in each of the coordinate directions. We observe a rate of convergence in the L_2-error norm of the velocity field that lies between quadratic and cubic. For a discretization of a classical Navier–Stokes problem using the isoparametric quadratic shape functions, a cubic rate is optimal; cf. Hughes [12]. Figure 5 juxtaposes the solution (49) and the finite-element approximation $\mathbf{v}^h$ obtained using a 4×4 uniform mesh. The latter is shown above the midplane $y/h = 0.5$ and the numerical approximation is seen to be indistinguishable from the solution.

For the pressure field, we obtain nearly a quadratic rate of convergence in the L_2 norm of $\mathbf{e}_p$. We are not aware of any studies detailing the accuracy of the pressure approximation for the mixed formulation described herein. However, this rate is above that expected based on the best approximation error for a linear field.

The accuracy and rate of convergence in the velocity and pressure fields was found to be sensitive to the particular choice of the stability terms τ_v and τ_p. Without any stabilization, for example, we observed much lower accuracy in both fields. The results shown were obtained using τ_p and τ_v proportional to ζ/h_e where h_e denotes the width of the element edges. Such a scaling with mesh spacing is likely the minimum requirement to maintain convergence, and is consistent with error estimates provided in Engel et al. [8]. We anticipate that much better results could be obtained using stabilization parameters that are more closely related to the solution. This is an area for future work.

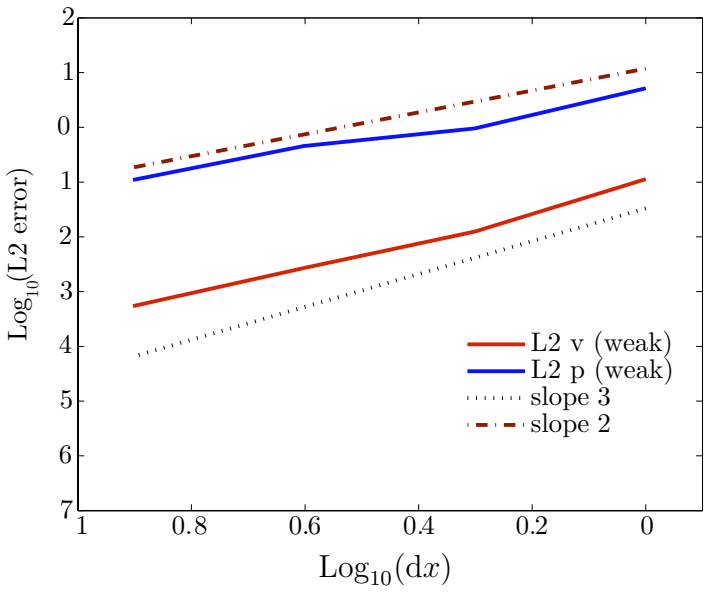

Fig. 4. Convergence results for the benchmark problem for weak adherence boundary conditions.

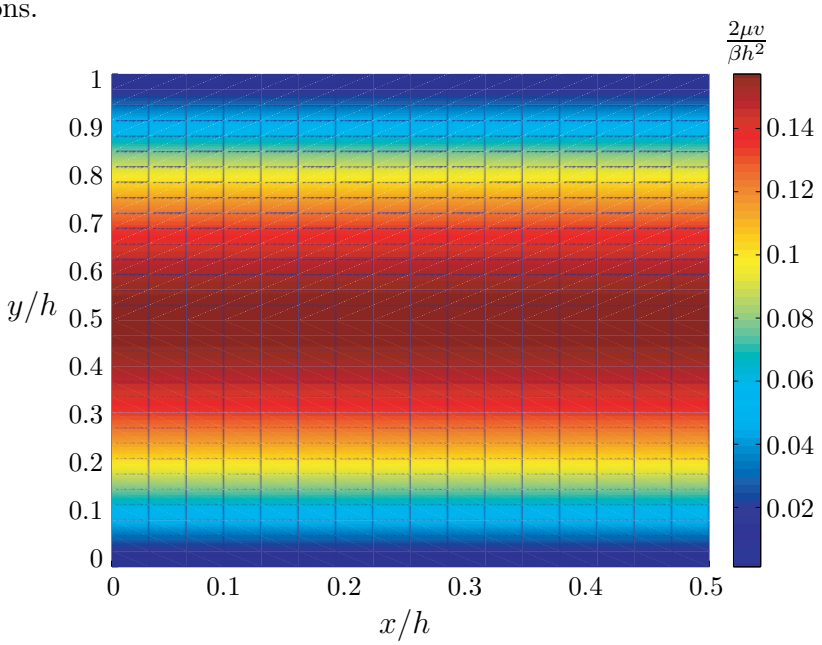

Fig. 5. Contour plot of velocity field normalized by $\beta h^2/2\mu$ for weak adherence boundary conditions. The finite-element approximation is shown above the channel center $y/h = 0.5$ and the solution (49) is shown below this line.

Figure 6 compares numerical and exact solutions for the case of generalized adherence conditions ($l > 0$) on the channel wall, using various ratios l/L of adherence length to gradient length. The numerical results were obtained at the outflow ($x/h = 0.5$) boundary of the computational domain. All of the numerical results shown in Figure 6 are for a uniform mesh of 4×4 elements. The results indicate an excellent match between the numerical and exact velocity fields, particularly given the coarseness of the mesh. Figure 7 shows the

contours of the normalized pressure gradient obtained for the particular choice of $l/L = 0.1$. As expected, the pressure gradient is almost constant and the maximum error is less than 3%.

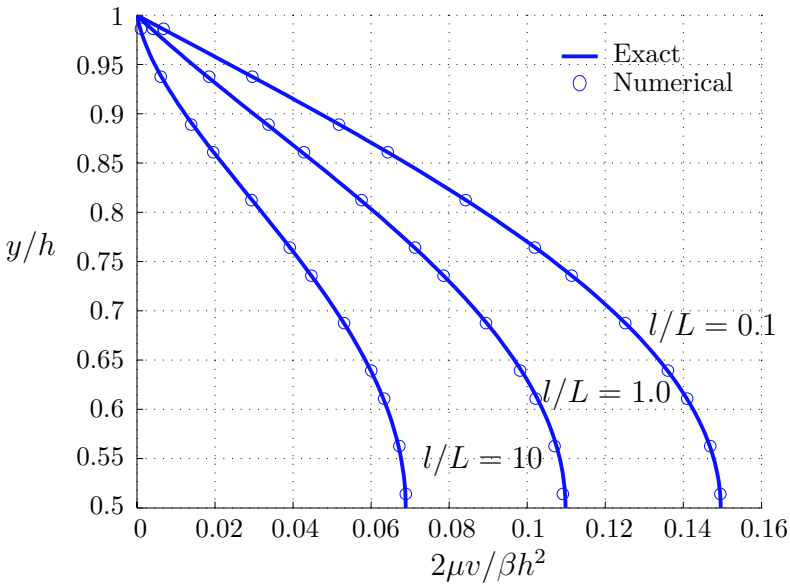

Fig. 6. Exact and numerical velocity profiles at the outlet boundary of the computational domain for various ratios l/L of adherence length to gradient length. All numerical results were obtained on a 4×4 uniform mesh.

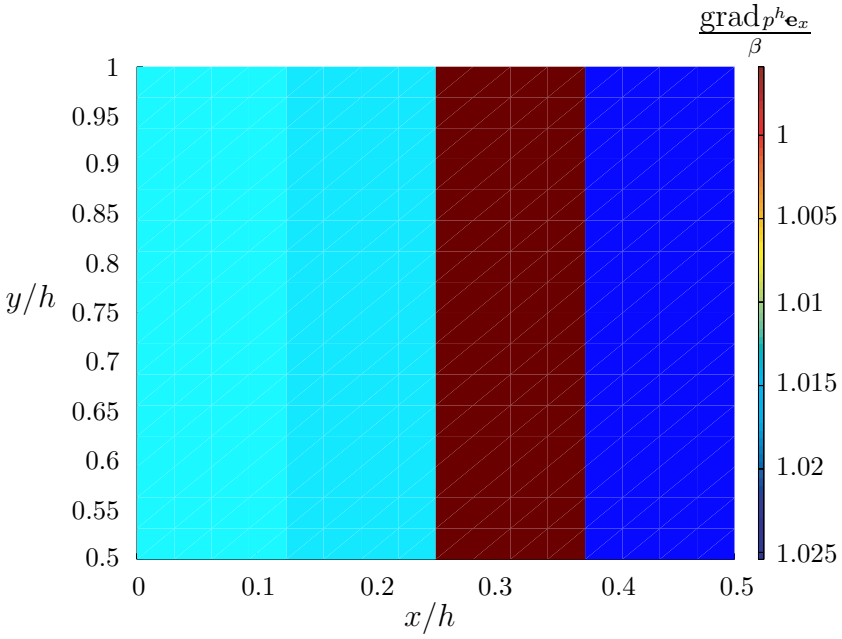

Fig. 7. Contour plot of the normalized pressure gradient $\mathbf{e}_x \cdot \text{grad}\, p^h/\beta$ for channel flow with generalized adherence boundary conditions ($l/L = 1.0$).

A convergence study with generalized adherence boundary conditions on the

channel walls yields results that are qualitatively similar to those arising for weak adherence boundary conditions. Figure 8 compares the relative error norms for the two cases. The generalized adherence results were obtained using $l/L = 0.1$. We report that the rates of convergence are nearly unaffected with generalized adherence boundary conditions, and a slight increase in accuracy was observed with increasing mesh refinement.

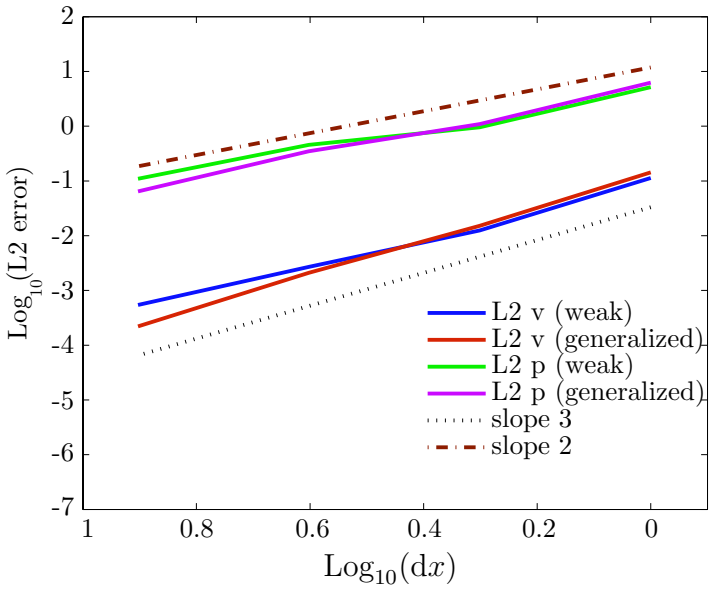

Fig. 8. Convergence results for the benchmark problem for weak and generalized adherence boundary conditions.

As a final verification test, we report results using skewed meshes. Figure 9 shows velocity contours for the case of generalized adherence boundary conditions with the skewed mesh geometry superimposed over the finite-element approximation to $\mathbf{v}$. The numerical results once again compare favorably to the solution.

We note that this benchmark problem also permits us to examine other choices for boundary conditions and their effect on the numerical solution. Heywood et al. [13] proposed a simple method to prescribe a pressure drop between artificial inlet and outlet boundaries such as the left and right boundaries in Figure 3. Writing $-P$ for the desired pressure drop between the artificial inlet and outlet boundaries, the approach amounts to replacing the prescribed velocity boundary condition at the inlet with a traction

$$\mathbf{t} = -P\mathbf{e}_x. \tag{51}$$

Using such an approach, we obtain nearly identical results to those obtained using the boundary conditions described in Figure 2. This approach will be used in Section 5.3 to study flow through a channel with a step.

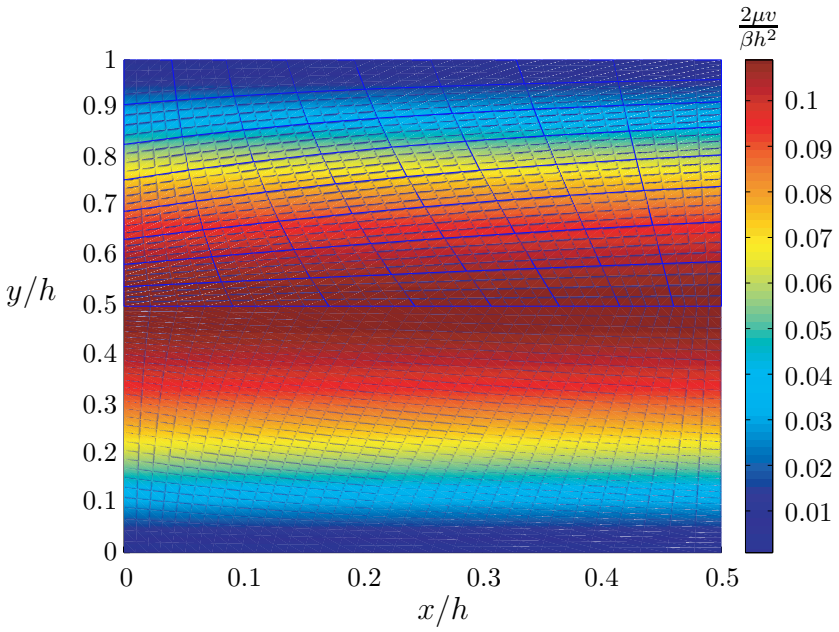

Fig. 9. Contour plot of velocity field normalized by $\beta h^2/2\mu$ for generalized adherence boundary conditions, with $l/L = 1.0$. The finite-element approximation and smoothed mesh is shown above the channel center $y/h = 0.5$ and the solution (49) is shown below this line.

5.2 Flow Past a Cylinder

The second benchmark problem that we consider involves steady, laminar flow past a right circular cylinder. We consider a domain of height h and width w containing a circular obstacle of diameter d (Figure 10). The boundary conditions for the hypertraction $\mathbf{m}_s$ and the horizontal and vertical components u and v of the velocity field are indicated in the Figure. On the cylinder surface, no slip conditions are considered along with generalized adherence boundary conditions ($l > 0$). A uniform velocity in the x-direction at the inlet boundary is applied. The computational domain is taken as $h/w = 1$, and $h/d = 4$. We find that the mesh shown in Figure 11 of 288 quadratic elements provides sufficiently converged results for all of the problems presented below.

Figure 12 compares numerical approximations for the horizontal component of the velocity field for the classical Navier–Stokes theory and the gradient theory. The results correspond to generalized adherence boundary conditions ($l > 0$) on the cylinder surface, with $L/d = 1.0$ and $l/L = 10.0$. The two solutions are seen to be qualitatively quite similar, with perhaps the greatest difference occurring in the vicinity of the cylinder. This is not surprising given the generalized adherence condition there.

Figure 13 displays contour plots of the vertical component of the velocity field for the classical Navier–Stokes theory and the gradient theory. Only minor qualitative and quantitative differences between the two flows can be observed,

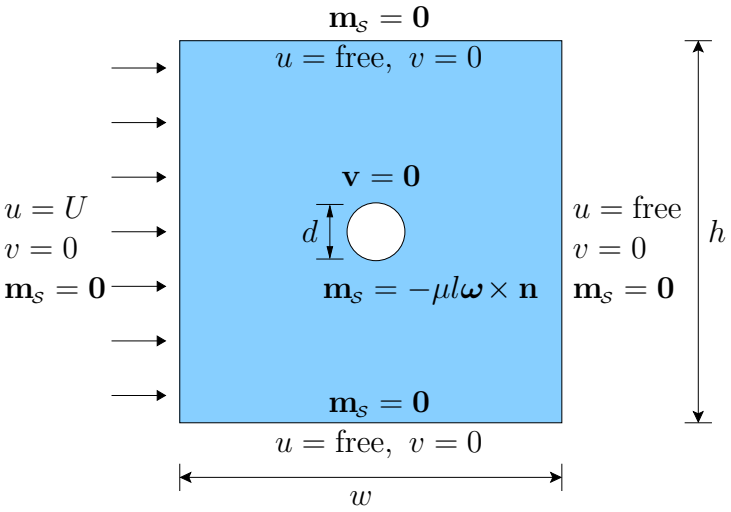

Fig. 10. Problem description for flow past a cylinder with velocity and hypertraction boundary conditions.

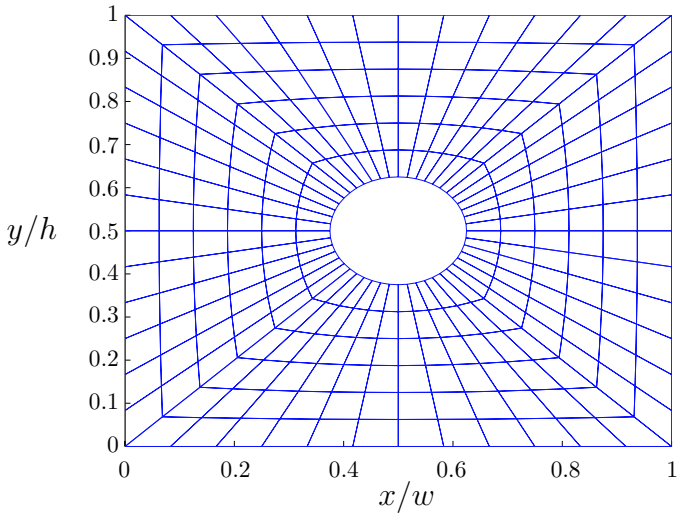

Fig. 11. Mesh for studies of flow past a cylinder.

but the adherence near the cylinder boundary is clearly identifiable. Figure 14 shows the pressure distributions for the classical (left) and gradient (right) flows. As expected, these results show a pressure drop as the flows pass the cylinder. Moreover, we find that the pressure field upstream of the cylinder for the gradient theory is greater than that predicted by the classical theory.

Figure 15 compares the horizontal velocity components for the classical theory with those of weak- and generalized- adherence boundary conditions under the gradient theory. The numerical results correspond to the flow profiles along a vertical line along the middle ($x/h = 0.5$) of the computational domain. All of the numerical results shown in the Figure were obtained using a mesh of 288 elements. The results indicate that the velocity profiles at small length

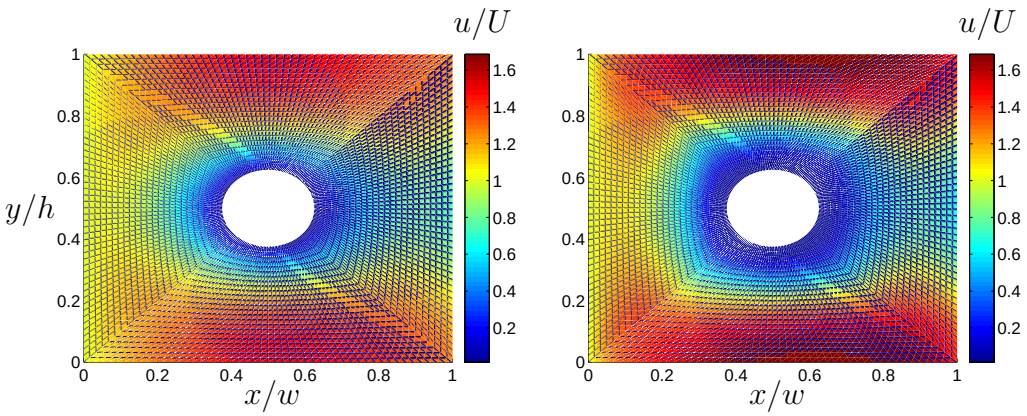

Fig. 12. Contour plots of the normalized horizontal velocity component for the classical theory (left) and the gradient theory (right) with generalized adherence boundary conditions. Results for the gradient theory correspond to $L/d = 1.0$ and $l/L = 10.0$.

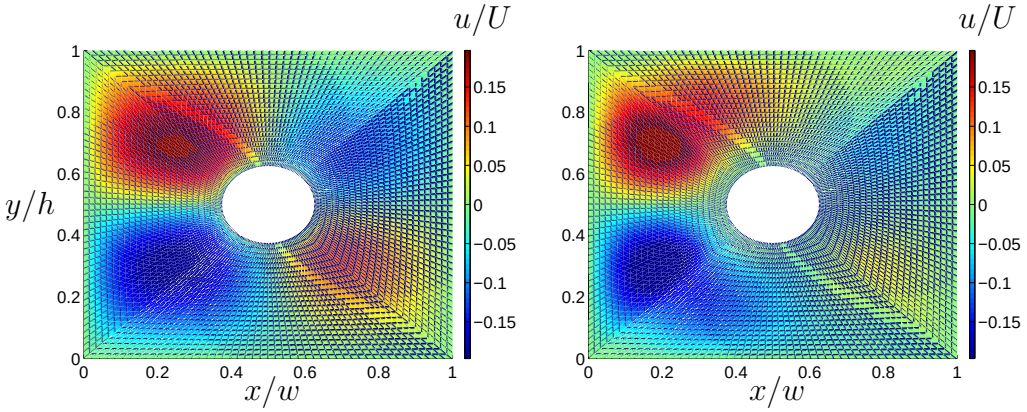

Fig. 13. Contour plots of the normalized vertical velocity component for the classical solution (left) and the gradient (right) solution with generalized adherence boundary conditions. Results for the gradient theory correspond to $L/d = 1.0$ and $l/L = 10.0$.

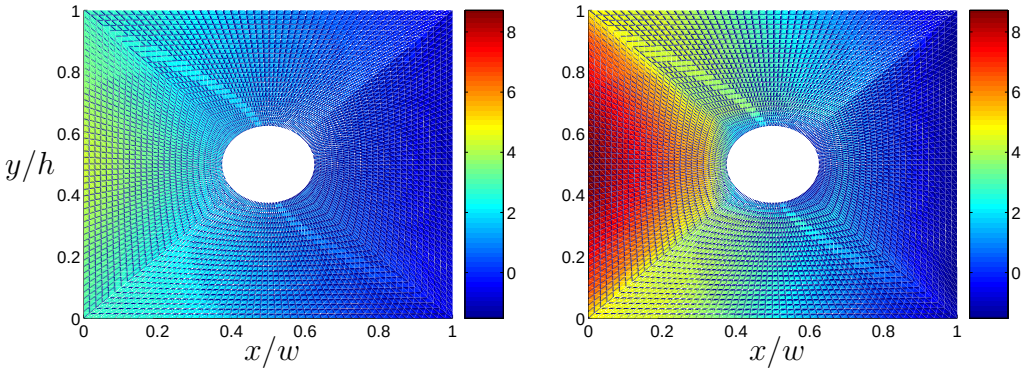

Fig. 14. Contour plots of pressure field for the classical solution (left) and the gradient (right) solution with generalized adherence boundary conditions.

scales are smaller than those of classical theory. Moreover, the slope around the cylinder decreases with increasing gradient and adherence lengths (L and l).

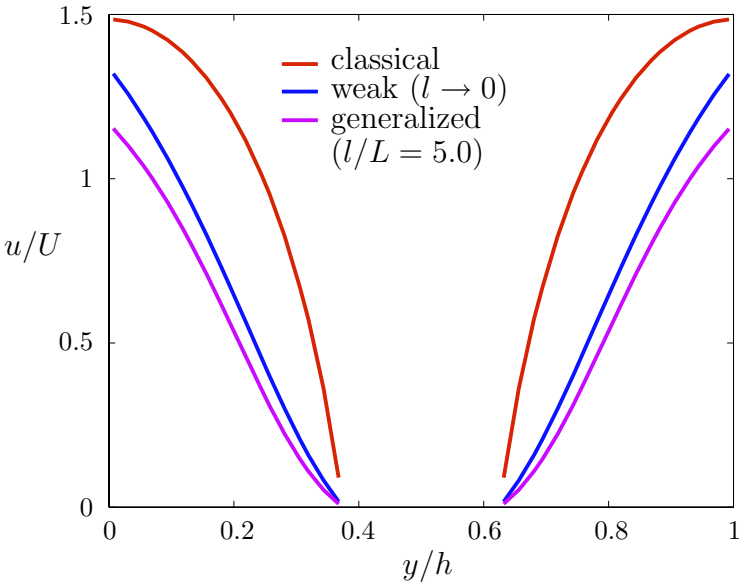

Fig. 15. Comparison of the normalized horizontal velocity component profiles in the middle ($x/w = 0.5$) of the computational domain for the classical theory and weak- and generalized-adherence boundary conditions on the cylinder surface with the gradient theory.

5.3 Step Flow

We consider a steady, laminar flow through a channel with a sudden area expansion as shown in Figure 16. We prescribe a pressure drop $-P$ between the inlet and outlet boundaries as shown in the Figure. The vertical component of the velocity field is also fixed to zero at the inlet and outlet boundaries. On the top and bottom surfaces, no-slip boundary conditions are enforced, and weak adherence ($l = 0$) conditions are considered for the gradient theory. The dimensions of the computational domain are taken such that $w_1/w_2 = 3$, $h_1/h_2 = 5/2$, and $h_1/w_1 = 5/6$.

Figure 17 and 18 provide contour plots of the numerical solution of the horizontal and vertical velocity components for classical (left) and gradient (right) flows. The numerical results were obtained using a uniform mesh of 176 elements. As expected, the results reveal a qualitative difference between classical and gradient theories. Figure 19 provides the pressure comparison at the same contour level between classical and gradient theories. The results clearly show the same net pressure drop between inlet and outlet boundaries. A profile of the horizontal velocity field at the outlet of the computational domain is shown

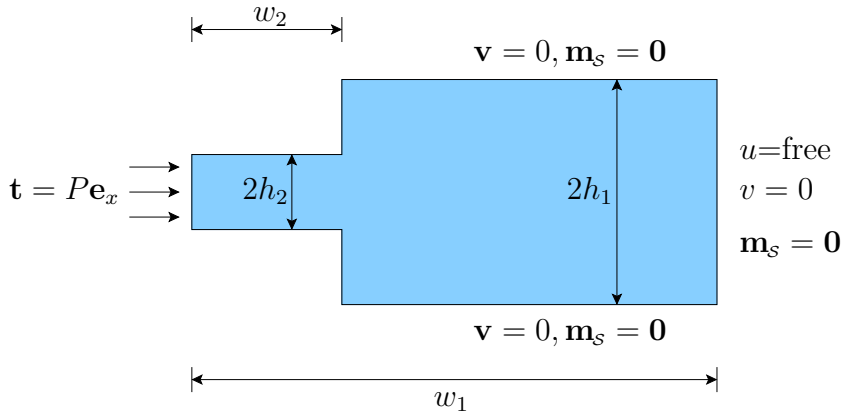

Fig. 16. Geometry and boundary conditions for the step flow problem. The coordinates in the directions downstream and out of the plane are x and z.

in Figure 20. The gradient theory clearly predicts smaller flow rates compared to the classical for the same pressure drop across the step. The results for the gradient theory shown in Figures 17–20 were all obtained using $L/h_2 = 0.25$.

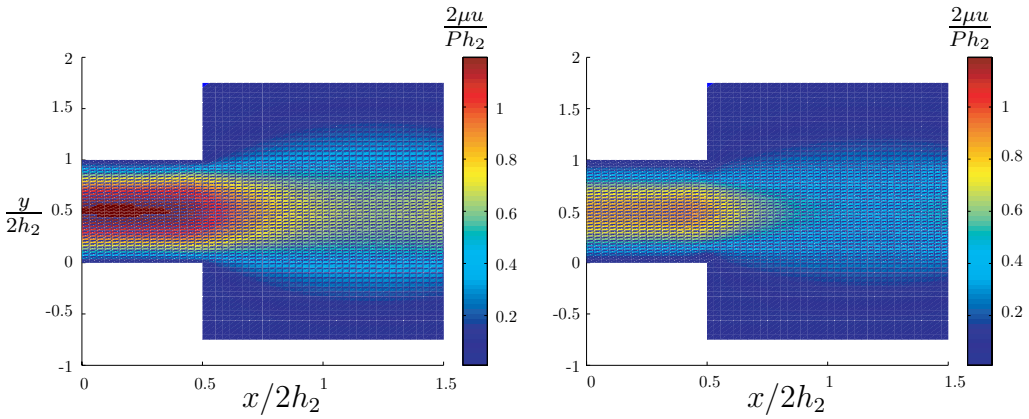

Fig. 17. Contour plot of normalized horizontal velocity component predicted using the classical theory (left) and the gradient theory (right) with weak adherence boundary conditions.

We next examine the variation in flow rates with aspect ratio h_1/h_2 for a fixed pressure drop. We calculate the flow rates Q for a sequence of steps ranging from $h_1 = h_2$ (the straight channel) to $h_1 = 2.5h_2$. We use the flow rate Q_1 obtained for the straight channel in each case (classical and gradient) to normalize the subsequent results. Figure 21 shows the normalized flow rates as a function of step ratio h_1/h_2 for a sequence of increasing ratios L/h_2 of gradient to physical lengths. The results predict that the flow rate of the classical theory is always greater than that of the gradient theory. Moreover,

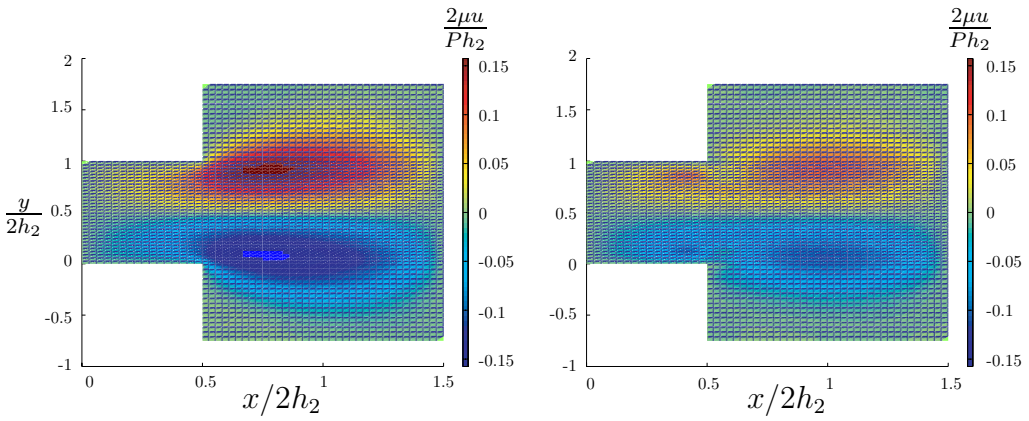

Fig. 18. Contour plot of vertical velocity component for the classical solution (left) and the gradient (right) solution with weak adherence boundary conditions.

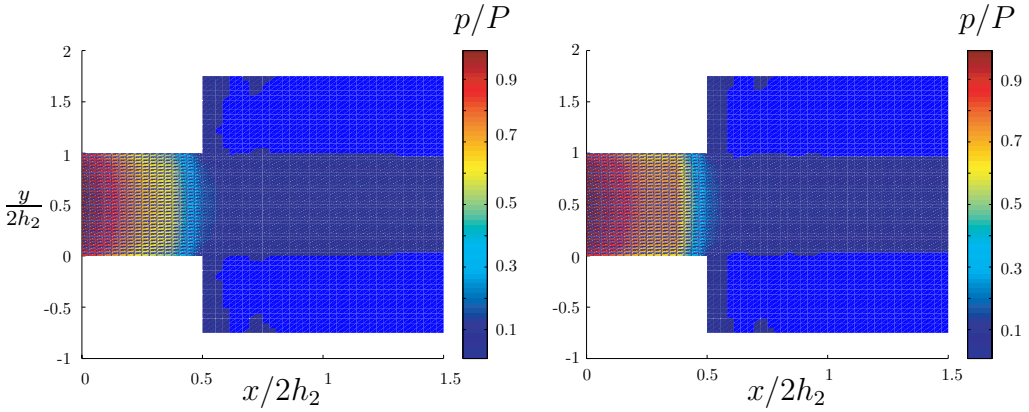

Fig. 19. Contour plot of normalized pressure fields for the classical (left) and gradient (right) theories for the step flow problem.

flow rates are seen to decrease relative to the straight channel rate as the gradient length is increased relative to the physical length. We note that the introduction of the corner to the problem results in a marked decrease in flow rates (before a more gradual increase with increasing step size) for large L/h_2. This may be attributable to the increased role that corner singularities may play with regard to dissipation for the gradient theory.

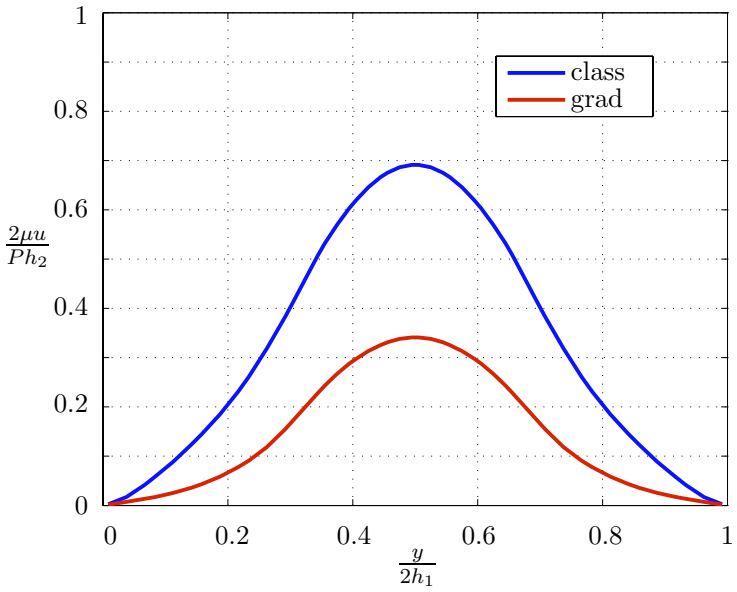

Fig. 20. Normalized horizontal velocity profiles at the outlet of the computational domain for the classical theory and the gradient theory for the step flow problem.

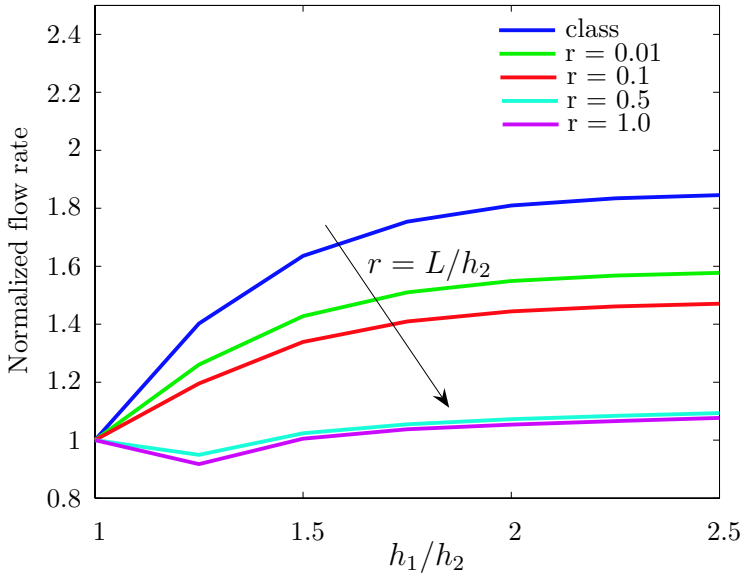

Fig. 21. Normalized flow rates as a function of step ratio h_1/h_2 for a sequence of increasing ratios L/h_2 of gradient to physical lengths.

6 Summary and Conclusions

In this paper, we described a finite-element method for a second-gradient theory of fluid flow. The second gradient theory incorporates gradients of the vorticity field that are power-conjugate to a hyperstress in a nonstandard principle of virtual power. The theory gives rise to a flow equation that is fourth-order in the velocity field, and incorporates associated higher-order boundary conditions. Rather than employing C^1-continuous basis functions or a fully mixed

approach, we base our method on a recent formulation for fourth-order elliptic problems that employs C^0-continuous basis functions. Continuity of higher-order velocity derivatives is then enforced between elements using a variation of Nitsche's [10] method, involving jump quantities across interelement boundaries. Using this formulation, we based our approach on second-order elements that are stable for the classical Navier-Stokes theory for incompressible fluid flow. Additional terms were added to properly stabilize the discontinuous pressure field.

Using our finite-element method, we then examined several numerical examples. First, the method was verified using an analytical solution to a Poiseuille flow problem derived by Fried and Gurtin [4]. An excellent match between numerical and analytical results was obtained, as were near-optimal rates of convergence in appropriate error norms for the velocity and pressure fields. The numerical method was also shown capable of capturing effects for a range of boundary conditions stemming from the second-gradient theory, from weak to strong adherence. Results were obtained using stabilization parameters that scale with the second-gradient moduli and the inverse of the mesh spacing. Additional problems of flow past a cylinder and step flow were then examined, and numerical predictions based on the second-gradient theory were compared to those of the classical theory. Consistent with the additional sources of dissipation associated with the hyperstress and the generalized adherence boundary conditions, the second-gradient theory predicts lower flow rates and shows a marked difference near boundaries due to the effect of the adherence boundary conditions.

This work is based on a theory of fluid flow that involves the gradient of the vorticity field [5]. It shares several common features with an earlier theory based on the full second-gradient of the velocity field [4]. The earlier theory involves an additional hyperpressure field not present in the vorticity-based theory considered here. A numerical formulation based on the earlier theory would thus require a three-field approach that would be more difficult to ensure stability. Since both theories yield identical flow equations, however, we do not anticipate significant qualitative differences in the flow profiles.

Future work will focus on extending our approach to time-dependent flows beyond the steady Stokes flows considered herein. This work should serve as an excellent starting point for a formulation based on the generalization of the LANS-α theory for turbulent flow obtained by Fried and Gurtin [5], for example. Importantly, we intend to examine methods that can better tie the stabilization parameters to the solution in a particular problem. Along these lines, Mourad et al. [14] have recently developed a method to relate the stabilization parameters in Nitsche's [10] method to the relationship between coarse and fine scales in a solution. In principle, such a strategy could be applied to the present work, provided that a suitable approximation for the

fine-scale can be identified.

Acknowledgements

The support of the Department of Energy to Duke University and Washington University is gratefully acknowledged.

References

[1] M. E. Gurtin, A gradient theory of single-crystal viscoplasticity that accounts for geometrically necessary dislocations, *J. Mech. Phys. Solids* **84** (2001), 809–819.

[2] R. A. Toupin, Elastic materials with couple stresses, *Arch. Ration. Mech. Anal.* **11** (1962), 385–414.

[3] R. A. Toupin, Elastic materials with couple stresses, *Arch. Ration. Mech. Anal.* **17** (1964), 85–112.

[4] E. Fried and M. E. Gurtin, Tractions, balances, and boundary conditions for nonsimple materials with application to liquid flow at small length scales, *Arch. Ration. Mech. Anal.* (2006), in press.

[5] E. Fried and M. E. Gurtin, Cosserat fluids and the continuum mechanics of turbulence: a generalized Navier–Stokes-α equation with complete boundary conditions, *Submitted for publication* (2006).

[6] J. Petera and J. F. T. Pittman, Isoparametric hermite elements, *Int. J. Num. Meth. Engrg.* **37** (1994), 3489–3519.

[7] M. Fortin and F. Brezzi, Mixed and hybrid finite element methods, Springer, New York, (1991).

[8] G. Engel, K. Garikipati, T. J. R. Hughes, M. G. Larson, L. Mazzei and R. L. Taylor, Continuous/discontinuous finite element approximations of fourth-order elliptic problems in structural and continuum mechanics with applications to thin beams and plates, and strain gradient elasticity, *Comput. Meth. Appl. Mech. Engrg.* **191** (2002), 3669–3750.

[9] T. J. R. Hughes, *The Finite Element Method* Dover Publications, New York, 1987.

[10] J. A. Nitsche, Über ein Variationsprinzip zur Lösung von Dirichlet-Problemen bei Verwendung von Teilräumen, die keinen Randbedingungen unterworfen sind. *Abhandlungen aus dem Mathematischen Seminar der Universität Hamburg* 1970/71; **36**:9–15.

[11] T. J. R. Hughes and L. P. Franca, A new finite element formulation for computational fluid dynamics: VII, *Comp. Meth. Appl. Mech. Eng.* **65** (1987), 85–96.

[12] T. J. R. Hughes, L. P. Franca and M. Balestra, A new finite element formulation for computational fluid dynamics: V. Circumventing the Babuska-Brezzi condition: a stable Petrov-Galerkin formulation of the Stokes problem accommodating equal-order interpolations, *Comp. Meth. Appl. Mech. Engrg.* **59** (1986), 85–99.

[13] J. G. Heywood, S. Rannacher and S. Turek, Artificial boundaries and flux and pressure conditions for the incompressible Navier–Stokes equations, *Int. J. Num. Meth. Fluids* **22** (1996), 325–352.

[14] H. M. Mourad, J. Dolbow and I. Harari, A bubble-stabilized finite element method for Dirichlet constraints on embedded interfaces, *Int. J. Num. Meth. Engrg.* (2006), accepted for publication.

List of Recent TAM Reports

No.	Authors	Title	Date
1009	Bagchi, P., and S. Balachandar	Effect of turbulence on the drag and lift of a particle—*Physics of Fluids*, in press (2003)	Oct. 2002
1010	Zhang, S., R. Panat, and K. J. Hsia	Influence of surface morphology on the adhesive strength of aluminum/epoxy interfaces—*Journal of Adhesion Science and Technology* **17**, 1685–1711 (2003)	Oct. 2002
1011	Carlson, D. E., E. Fried, and D. A. Tortorelli	On internal constraints in continuum mechanics—*Journal of Elasticity* **70**, 101–109 (2003)	Oct. 2002
1012	Boyland, P. L., M. A. Stremler, and H. Aref	Topological fluid mechanics of point vortex motions—*Physica D* **175**, 69–95 (2002)	Oct. 2002
1013	Bhattacharjee, P., and D. N. Riahi	Computational studies of the effect of rotation on convection during protein crystallization—*International Journal of Mathematical Sciences* **3**, 429–450 (2004)	Feb. 2003
1014	Brown, E. N., M. R. Kessler, N. R. Sottos, and S. R. White	*In situ* poly(urea-formaldehyde) microencapsulation of dicyclopentadiene—*Journal of Microencapsulation* (submitted)	Feb. 2003
1015	Brown, E. N., S. R. White, and N. R. Sottos	Microcapsule induced toughening in a self-healing polymer composite—*Journal of Materials Science* (submitted)	Feb. 2003
1016	Kuznetsov, I. R., and D. S. Stewart	Burning rate of energetic materials with thermal expansion—*Combustion and Flame* (submitted)	Mar. 2003
1017	Dolbow, J., E. Fried, and H. Ji	Chemically induced swelling of hydrogels—*Journal of the Mechanics and Physics of Solids*, in press (2003)	Mar. 2003
1018	Costello, G. A.	Mechanics of wire rope—Mordica Lecture, Interwire 2003, Wire Association International, Atlanta, Georgia, May 12, 2003	Mar. 2003
1019	Wang, J., N. R. Sottos, and R. L. Weaver	Thin film adhesion measurement by laser induced stress waves—*Journal of the Mechanics and Physics of Solids* (submitted)	Apr. 2003
1020	Bhattacharjee, P., and D. N. Riahi	Effect of rotation on surface tension driven flow during protein crystallization—*Microgravity Science and Technology* **14**, 36–44 (2003)	Apr. 2003
1021	Fried, E.	The configurational and standard force balances are not always statements of a single law—*SIAM Journal on Applied Mathematics* **66**, 1130–1149 (2006)	Apr. 2003
1022	Panat, R. P., and K. J. Hsia	Experimental investigation of the bond coat rumpling instability under isothermal and cyclic thermal histories in thermal barrier systems—*Proceedings of the Royal Society of London A* **460**, 1957–1979 (2003)	May 2003
1023	Fried, E., and M. E. Gurtin	A unified treatment of evolving interfaces accounting for small deformations and atomic transport: grain-boundaries, phase transitions, epitaxy—*Advances in Applied Mechanics* **40**, 1–177 (2004)	May 2003
1024	Dong, F., D. N. Riahi, and A. T. Hsui	On similarity waves in compacting media—*Horizons in World Physics* **244**, 45–82 (2004)	May 2003
1025	Liu, M., and K. J. Hsia	Locking of electric field induced non-180° domain switching and phase transition in ferroelectric materials upon cyclic electric fatigue—*Applied Physics Letters* **83**, 3978–3980 (2003)	May 2003
1026	Liu, M., K. J. Hsia, and M. Sardela Jr.	In situ X-ray diffraction study of electric field induced domain switching and phase transition in PZT-5H—*Journal of the American Ceramics Society* (submitted)	May 2003
1027	Riahi, D. N.	On flow of binary alloys during crystal growth—*Recent Research Development in Crystal Growth* **3**, 49–59 (2003)	May 2003
1028	Riahi, D. N.	On fluid dynamics during crystallization—*Recent Research Development in Fluid Dynamics* **4**, 87–94 (2003)	July 2003
1029	Fried, E., V. Korchagin, and R. E. Todres	Biaxial disclinated states in nematic elastomers—*Journal of Chemical Physics* **119**, 13170–13179 (2003)	July 2003
1030	Sharp, K. V., and R. J. Adrian	Transition from laminar to turbulent flow in liquid filled microtubes—*Physics of Fluids* (submitted)	July 2003

List of Recent TAM Reports (cont'd)

No.	*Authors*	*Title*	*Date*
1031	Yoon, H. S., D. F. Hill, S. Balachandar, R. J. Adrian, and M. Y. Ha	Reynolds number scaling of flow in a Rushton turbine stirred tank: Part I—Mean flow, circular jet and tip vortex scaling—*Chemical Engineering Science* (submitted)	Aug. 2003
1032	Raju, R., S. Balachandar, D. F. Hill, and R. J. Adrian	Reynolds number scaling of flow in a Rushton turbine stirred tank: Part II—Eigen-decomposition of fluctuation—*Chemical Engineering Science* (submitted)	Aug. 2003
1033	Hill, K. M., G. Gioia, and V. V. Tota	Structure and kinematics in dense free-surface granular flow—*Physical Review Letters* **91**, 064302 (2003)	Aug. 2003
1034	Fried, E., and S. Sellers	Free-energy density functions for nematic elastomers—*Journal of the Mechanics and Physics of Solids* **52**, 1671–1689 (2004)	Sept. 2003
1035	Kasimov, A. R., and D. S. Stewart	On the dynamics of self-sustained one-dimensional detonations: A numerical study in the shock-attached frame—*Physics of Fluids* (submitted)	Nov. 2003
1036	Fried, E., and B. C. Roy	Disclinations in a homogeneously deformed nematic elastomer—*Nature Materials* (submitted)	Nov. 2003
1037	Fried, E., and M. E. Gurtin	The unifying nature of the configurational force balance—*Mechanics of Material Forces* (P. Steinmann and G. A. Maugin, eds.), 25–32 (2005)	Dec. 2003
1038	Panat, R., K. J. Hsia, and J. W. Oldham	Rumpling instability in thermal barrier systems under isothermal conditions in vacuum—*Philosophical Magazine*, in press (2004)	Dec. 2003
1039	Cermelli, P., E. Fried, and M. E. Gurtin	Sharp-interface nematic–isotropic phase transitions without flow—*Archive for Rational Mechanics and Analysis* **174**, 151–178 (2004)	Dec. 2003
1040	Yoo, S., and D. S. Stewart	A hybrid level-set method in two and three dimensions for modeling detonation and combustion problems in complex geometries—*Combustion Theory and Modeling* (submitted)	Feb. 2004
1041	Dienberg, C. E., S. E. Ott-Monsivais, J. L. Ranchero, A. A. Rzeszutko, and C. L. Winter	Proceedings of the Fifth Annual Research Conference in Mechanics (April 2003), TAM Department, UIUC (E. N. Brown, ed.)	Feb. 2004
1042	Kasimov, A. R., and D. S. Stewart	Asymptotic theory of ignition and failure of self-sustained detonations—*Journal of Fluid Mechanics* (submitted)	Feb. 2004
1043	Kasimov, A. R., and D. S. Stewart	Theory of direct initiation of gaseous detonations and comparison with experiment—*Proceedings of the Combustion Institute* (submitted)	Mar. 2004
1044	Panat, R., K. J. Hsia, and D. G. Cahill	Evolution of surface waviness in thin films via volume and surface diffusion—*Journal of Applied Physics* (submitted)	Mar. 2004
1045	Riahi, D. N.	Steady and oscillatory flow in a mushy layer—*Current Topics in Crystal Growth Research*, in press (2004)	Mar. 2004
1046	Riahi, D. N.	Modeling flows in protein crystal growth—*Current Topics in Crystal Growth Research*, in press (2004)	Mar. 2004
1047	Bagchi, P., and S. Balachandar	Response of the wake of an isolated particle to isotropic turbulent cross-flow—*Journal of Fluid Mechanics* (submitted)	Mar. 2004
1048	Brown, E. N., S. R. White, and N. R. Sottos	Fatigue crack propagation in microcapsule toughened epoxy—*Journal of Materials Science* (submitted)	Apr. 2004
1049	Zeng, L., S. Balachandar, and P. Fischer	Wall-induced forces on a rigid sphere at finite Reynolds number—*Journal of Fluid Mechanics* (submitted)	May 2004
1050	Dolbow, J., E. Fried, and H. Ji	A numerical strategy for investigating the kinetic response of stimulus-responsive hydrogels—*Computer Methods in Applied Mechanics and Engineering* **194**, 4447–4480 (2005)	June 2004
1051	Riahi, D. N.	Effect of permeability on steady flow in a dendrite layer—*Journal of Porous Media*, in press (2004)	July 2004

List of Recent TAM Reports (cont'd)

No.	*Authors*	*Title*	*Date*
1052	Cermelli, P., E. Fried, and M. E. Gurtin	Transport relations for surface integrals arising in the formulation of balance laws for evolving fluid interfaces—*Journal of Fluid Mechanics* **544**, 339–351 (2005)	Sept. 2004
1053	Stewart, D. S., and A. R. Kasimov	Theory of detonation with an embedded sonic locus—*SIAM Journal on Applied Mathematics* (submitted)	Oct. 2004
1054	Stewart, D. S., K. C. Tang, S. Yoo, M. Q. Brewster, and I. R. Kuznetsov	Multi-scale modeling of solid rocket motors: Time integration methods from computational aerodynamics applied to stable quasi-steady motor burning—*Proceedings of the 43rd AIAA Aerospace Sciences Meeting and Exhibit* (January 2005), Paper AIAA-2005-0357 (2005)	Oct. 2004
1055	Ji, H., H. Mourad, E. Fried, and J. Dolbow	Kinetics of thermally induced swelling of hydrogels—*International Journal of Solids and Structures* **43**, 1878–1907 (2006)	Dec. 2004
1056	Fulton, J. M., S. Hussain, J. H. Lai, M. E. Ly, S. A. McGough, G. M. Miller, R. Oats, L. A. Shipton, P. K. Shreeman, D. S. Widrevitz, and E. A. Zimmermann	Final reports: Mechanics of complex materials, Summer 2004 (K. M. Hill and J. W. Phillips, eds.)	Dec. 2004
1057	Hill, K. M., G. Gioia, and D. R. Amaravadi	Radial segregation patterns in rotating granular mixtures: Waviness selection—*Physical Review Letters* **93**, 224301 (2004)	Dec. 2004
1058	Riahi, D. N.	Nonlinear oscillatory convection in rotating mushy layers—*Journal of Fluid Mechanics*, in press (2005)	Dec. 2004
1059	Okhuysen, B. S., and D. N. Riahi	On buoyant convection in binary solidification—*Journal of Fluid Mechanics* (submitted)	Jan. 2005
1060	Brown, E. N., S. R. White, and N. R. Sottos	Retardation and repair of fatigue cracks in a microcapsule toughened epoxy composite—Part I: Manual infiltration—*Composites Science and Technology* (submitted)	Jan. 2005
1061	Brown, E. N., S. R. White, and N. R. Sottos	Retardation and repair of fatigue cracks in a microcapsule toughened epoxy composite—Part II: *In situ* self-healing—*Composites Science and Technology* (submitted)	Jan. 2005
1062	Berfield, T. A., R. J. Ong, D. A. Payne, and N. R. Sottos	Residual stress effects on piezoelectric response of sol-gel derived PZT thin films—*Journal of Applied Physics* (submitted)	Apr. 2005
1063	Anderson, D. M., P. Cermelli, E. Fried, M. E. Gurtin, and G. B. McFadden	General dynamical sharp-interface conditions for phase transformations in viscous heat-conducting fluids—*Journal of Fluid Mechanics* (submitted)	Apr. 2005
1064	Fried, E., and M. E. Gurtin	Second-gradient fluids: A theory for incompressible flows at small length scales—*Journal of Fluid Mechanics* (submitted)	Apr. 2005
1065	Gioia, G., and F. A. Bombardelli	Localized turbulent flows on scouring granular beds—*Physical Review Letters*, in press (2005)	May 2005
1066	Fried, E., and S. Sellers	Orientational order and finite strain in nematic elastomers—*Journal of Chemical Physics* **123**, 044901 (2005)	May 2005
1067	Chen, Y.-C., and E. Fried	Uniaxial nematic elastomers: Constitutive framework and a simple application—*Proceedings of the Royal Society of London A* **462**, 1295–1314 (2006)	June 2005
1068	Fried, E., and S. Sellers	Incompatible strains associated with defects in nematic elastomers—*Journal of Chemical Physics* **124**, 024908 (2006)	Aug. 2005
1069	Gioia, G., and X. Dai	Surface stress and reversing size effect in the initial yielding of ultrathin films—*Journal of Applied Mechanics*, in press (2005)	Aug. 2005
1070	Gioia, G., and P. Chakraborty	Turbulent friction in rough pipes and the energy spectrum of the phenomenological theory—*Physical Review Letters* **96**, 044502 (2006)	Aug. 2005

List of Recent TAM Reports (cont'd)

No.	*Authors*	*Title*	*Date*
1071	Keller, M. W., and N. R. Sottos	Mechanical properties of capsules used in a self-healing polymer—*Experimental Mechanics* (submitted)	Sept. 2005
1072	Chakraborty, P., G. Gioia, and S. Kieffer	Volcán Reventador's unusual umbrella	Sept. 2005
1073	Fried, E., and S. Sellers	Soft elasticity is not necessary for striping in nematic elastomers—*Journal of Applied Physics*, in press (2006)	Sept. 2005
1074	Fried, E., M. E. Gurtin, and Amy Q. Shen	Theory for solvent, momentum, and energy transfer between a surfactant solution and a vapor atmosphere—*Physical Review E*, in press (2006)	Sept. 2005
1075	Chen, X., and E. Fried	Rayleigh–Taylor problem for a liquid–liquid phase interface—*Journal of Fluid Mechanics* (submitted)	Oct. 2005
1076	Riahi, D. N.	Mathematical modeling of wind forces—In *The Euler Volume* (Abington, UK: Taylor and Francis), in press (2005)	Oct. 2005
1077	Fried, E., and R. E. Todres	Mind the gap: The shape of the free surface of a rubber-like material in the proximity to a rigid contactor—*Journal of Elasticity* **80**, 97–151 (2005)	Oct. 2005
1078	Riahi, D. N.	Nonlinear compositional convection in mushy layers—*Journal of Fluid Mechanics* (submitted)	Dec. 2005
1079	Bhattacharjee, P., and D. N. Riahi	Mathematical modeling of flow control using magnetic fluid and field—In *The Euler Volume* (Abington, UK: Taylor and Francis), in press (2005)	Dec. 2005
1080	Bhattacharjee, P., and D. N. Riahi	A hybrid level set/VOF method for the simulation of thermal magnetic fluids—*International Journal for Numerical Methods in Engineering* (submitted)	Dec. 2005
1081	Bhattacharjee, P., and D. N. Riahi	Numerical study of surface tension driven convection in thermal magnetic fluids—*Journal of Crystal Growth* (submitted)	Dec. 2005
1082	Riahi, D. N.	Inertial and Coriolis effects on oscillatory flow in a horizontal dendrite layer—*Transport in Porous Media* (submitted)	Jan. 2006
1083	Wu, Y., and K. T. Christensen	Population trends of spanwise vortices in wall turbulence—*Journal of Fluid Mechanics* (submitted)	Jan. 2006
1084	Natrajan, V. K., and K. T. Christensen	The role of coherent structures in subgrid-scale energy transfer within the log layer of wall turbulence—*Physics of Fluids* (submitted)	Jan. 2006
1085	Wu, Y., and K. T. Christensen	Reynolds-stress enhancement associated with a short fetch of roughness in wall turbulence—*AIAA Journal* (submitted)	Jan. 2006
1086	Fried, E., and M. E. Gurtin	Cosserat fluids and the continuum mechanics of turbulence: A generalized Navier–Stokes-α equation with complete boundary conditions—*Journal of Fluid Mechanics* (submitted)	Feb. 2006
1087	Riahi, D. N.	Inertial effects on rotating flow in a porous layer—*Journal of Porous Media* (submitted)	Feb. 2006
1088	Li, F., and D. E. Leckband	Dynamic strength of adhesion surfaces—*Journal of Chemical Physics* (submitted)	Mar. 2006
1089	Chen, X., and E. Fried	Squire's theorem for the Rayleigh–Taylor problem with a phase transformation—*Proceedings of the Royal Society of London A* (submitted)	Mar. 2006
1090	Kim, T.-Y., J. Dolbow, and E. Fried	A numerical method for a second-gradient theory of incompressible fluid flow—*Journal of Computational Physics* (submitted)	Apr. 2006